Cooperative motion of domain walls in magnetic multilayers

Jason N. Armstrong, Susan Z. Hua, and Harsh Deep Chopra*
Laboratory for Quantum Devices, Materials Program, Department of Mechanical and Aerospace Engineering, State University of New York at Buffalo, Buffalo, New York 14260, USA

(Received 15 November 2010; revised manuscript received 6 January 2011; published 23 February 2011)

It is well known that the sequence of induced emf spikes in a Barkhausen spectrum bears no resemblance to the sequence of spikes in successive field cycles; in general, no two spectra are ever alike. The present study reports the observation of remarkably reproducible Barkhausen spectra over repeated field cycling in TbFe/FeCo exchange spring multilayers. Their reproducibility is shown to have origins in the highly synchronized and cooperative motion of domain walls in different layers. Whereas a handful of previous studies have shown limited reproducibility in small field excursions, in small samples, or over small distances, the reproducibility of magnetic avalanches in the present study occurs along the entire major magnetization loop, and the emf avalanches can be reproducibly transmitted over macroscopic distances (∼1 cm). The complexity of these highly reproducible spectra varies with the in-plane field direction, and reveals a new mode of magnetization reversal along the hard axis. Results also provide an avenue for information transmission over macroscopic distances in a magnetic medium.

DOI: 10.1103/PhysRevB.83.054426 PACS number(s): 75.60.Ej, 75.78.Fg

I. INTRODUCTION

Langmuir had originally predicted the existence of magnetic domain walls and a finite velocity for their propagation[1] to explain the observed dynamics of magnetization reversal,[2] a prediction that was subsequently confirmed by the classic works of Sixtus, Tonks, and Langmuir.[3–6] In a varying magnetic field, microscopic segments of domain walls randomly get pinned by defects. Locally, once the applied field exceeds the pinning force, the abrupt unpinning of wall segments causes sudden changes in flux $d\varphi$ within the microscopic volumes of the material. This rate of change of flux can be easily followed by an adjacent Faraday coil; the magnitude of induced emf ξ being proportional to the rate of change of flux with time $\xi\alpha -\frac{d\varphi}{dt}$. The resulting distribution of voltage spikes as a function of applied field is commonly referred to as the Barkhausen "spectrum."[2] In general, a cascade of voltage spikes occurs near the coercive fields $\pm H_c$ as a result of a large number of unpinning events in the material.[7–23]

One can thus view a domain wall as a microscopic "probe" of the magnetic medium as it moves in an applied field. Moreover, the use of such a probe is also not limited to studying wall-defect interactions only. For example, the induced emf caused by wall motion can be used to investigate wall velocity, wall mobility, its temperature dependence, damping, as well as temperature- or pressure-dependent spin reorientation.[3,4,17,24–37] Pertinent to the present study, motion of domain walls in a magnetic multilayer can also be used as a probe for interlayer coupling strength. This is because in multilayers, the magnetic behavior of one layer is influenced by other layers due to direct and/or indirect exchange interactions. The demagnetization of stray fields, emanating from domain walls in different layers, through interlayer flux closure is well known to reduce the domain-wall energy and increase the wall width, giving rise to new wall structures that are otherwise not possible in single films.[38–47] The overlapping walls in different layers reduce the overall energy by creating so-called *twin walls* that are comprised of Néel walls and quasi-Néel walls. The stray fields emanating from a Néel wall creates a magnetic disturbance in adjacent layers, causing their magnetization to locally rotate relative to the magnetization profile within the Néel wall, giving rise to so-called quasi-Néel walls; see Refs. 38 and 43–50 and references within for structure, energy, and observation of twin walls. This is shown, for example, in a TbFe/FeCo multilayer in Fig. 1(a) and schematically in Fig. 1(b). Depending on the strength of coupling, individual layers can either undergo reversal largely independent of each other (weak coupling), or in unison via the lock-step motion of a twin wall (strong coupling).[47] Whereas in certain applications it is desirable to purposely decouple different layers (as is the case, for example, in giant magnetoresistance spin valves[51–55] where the ferromagnetic "free" layer is deliberately decoupled with respect to the antiferromagnetically pinned ferromagnetic layers to maximize the magnetoresistance effect), in many other instances, the layers have to be coupled strongly to ensure a unified magnetization response. This, for example, is the case for giant magnetostriction TbFe-FeCo multilayers based on Kneller's exchange spring mechanism,[47,56–66] where weak coupling would cause the magnetostriction effect to diminish. Obviously in such multilayers, instead of independent motion of domain walls in individual layers, the *cooperative motion* of twin wall is more relevant and is the focus of the present study.

II. EXPERIMENTAL DETAILS

The TbFe/FeCo multilayers were deposited by magnetron sputtering on Si ⟨100⟩ substrates that were coated with a 6-nm Ta seed layer for better adhesion. The sputtering was carried out at 40 W in an Ar pressure of ∼3 mTorr in an ultrahigh vacuum chamber whose base pressure was $\sim 10^{-8}$ to 5×10^{-9} Torr. Samples were capped with an ∼2.5-nm-thick Au layer to prevent oxidation over time. The {TbFe (7 nm)/FeCo (10 nm)} films were deposited with number of bilayers ranging from 1 to 50; the TbFe was always the starting layer. The individual layer thickness is below the

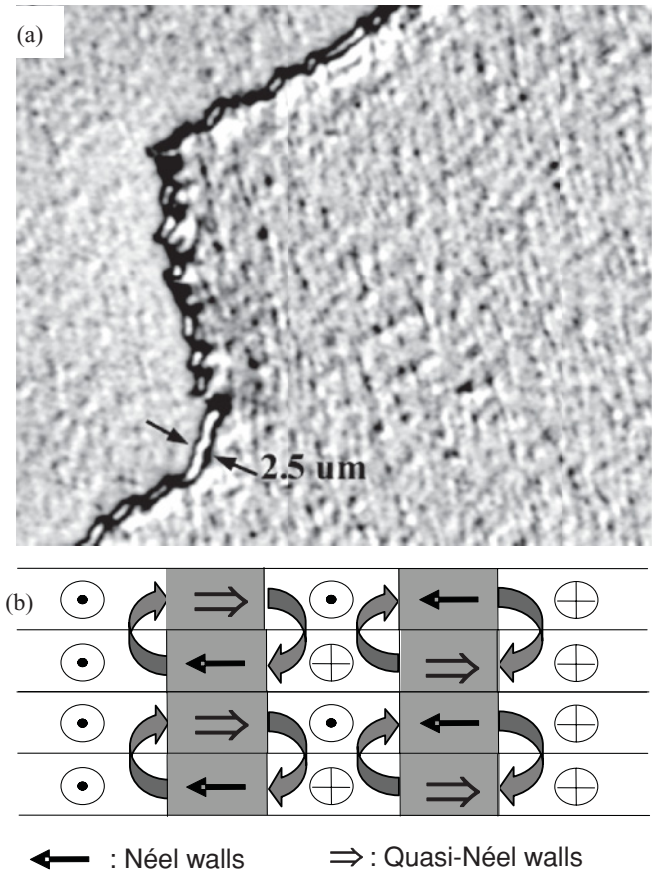

FIG. 1. (a) A twin domain wall in a {TbFe (7 nm)/FeCo (10 nm)} multilayer with two bilayers. (b) Schematic of the twin wall, which consists of Néel walls and quasi-Néel walls in different layers. See text for explanation.

domain-wall thickness to prevent formation of domain walls *parallel* to the interfaces, whose presence would otherwise lead to a more complex domain behavior (and reduced magnetostriction); the magnetoelastic behavior of similar films was discussed previously.[47,61,62] Magnetization curves were measured along different in-plane directions using a room-temperature vibrating sample magnetometer.

As shown in the following section, these multilayers undergo magnetization reversal by nucleation and motion of a *single* twin wall across the entire area of the samples, ~1.8 cm × ~1.8 cm, as opposed to nucleation and growth of multiple twin walls in different regions of the sample. The cooperative dynamics of the twin wall was detected by placing a miniaturized inductive pickup coil on the surface of the sample, as shown schematically in Fig. 2 (not drawn to scale). The sample and the pickup coil sits between the pole pieces of an electromagnet, and cycles between fields as high as ±2500 Oe, as dictated by the saturation characteristics of individual samples. The motion of the twin wall induces an emf signal, which is detected by the pickup coil. The signal is fed into a custom designed low-noise (~400–500 nV), two-stage voltage amplifier. The first stage of the amplifier has a gain of 5 K and the second stage has a gain of 10, for a total gain of 50 K. The amplified signal is then passed through a high-pass filter to remove the dc component of the signal,

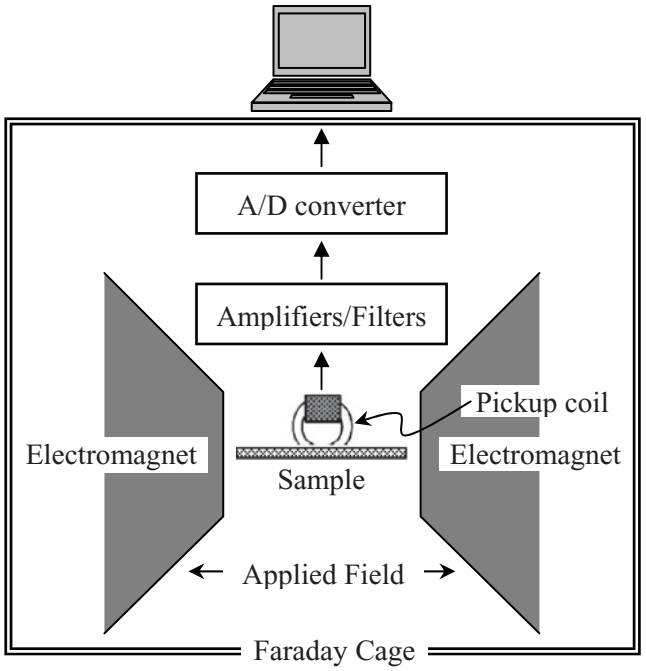

FIG. 2. Schematic of the experimental setup used to measure the Barkhausen signal.

followed by another filter that is bandwidth limited from 1 to 10 kHz. Batteries were used to power the circuit to ensure a clean supply. To minimize the influence of external noise, the entire assembly was placed inside a Faraday cage, as shown in Fig. 2. To measure the velocity of the wall as a function of driving rate, two similar pickup coils were placed on the sample 1 cm apart. The time taken by the wall to move this distance can then be used to measure the wall velocity. To ensure that the same wall is being traversed across both pickup coils, the polarity of one coil was reversed relative to the other to deliberately invert the sign of the induced emf signal in one coil relative to the other. In addition, emf experiments with *in situ* micromagnetic observations were also done, which provided direct confirmation of reversal in the entire sample by a single twin wall.

The micromagnetic structure was studied using the high-resolution interference contrast colloid (ICC) method,[67] and is described in detail elsewhere.[61,68–71] Briefly, the ICC method employs a colloidal solution to decorate the microfield on a magnetic surface, similar to the versatile Bitter method.[72] However, the technique differs in the manner in which the colloid decorated microfield is detected. In the Bitter method, a problem in contrasts develops in the bright-field or the dark-field mode due to backscattering by particles and various surfaces between the objective lens and the specimen, which results in an overall loss of resolution. Instead, the ICC method uses a Nomarski interferometer to detect the surface microfield distribution. The magnetic microfield on the surface causes local variation in the density of colloid particles (the average colloid particle size is 7 nm), thereby delineating the domain structure. This microfield is detected by polarization interferometer optics, which detects any unevenness at the nanometer scale and reveals domain structure with a pronounced three-dimensional effect and at a

high resolution that is limited only by that of the microscope (∼0.4–0.6 μm). In-plane magnetic field was applied by placing the sample between the pole pieces of an electromagnet. For domain imaging, samples were first saturated in either positive or negative field, followed by a decrease in field strength to zero and then cycled in the opposite direction. The domain observation system is automated and interfaced with an image frame grabber and a data acquisition card (for applied field). The experimental setup acquires and labels all images and data automatically. The software operating the acquisition card has the ability to embed important experimental information directly on the records, which are automatically collated and numbered as image galleries for subsequent analysis as "virtual experiments."

III. RESULTS

Figures 3(a) and 3(b) show, respectively, the angular dependence of in-plane remanence and coercivity in a TbFe/FeCo film with 50 bilayers. The angular dependence of remanence in Fig. 3(a) is similar to that of a film with uniaxial anisotropy, *viz.*, maxima along the easy axes [90° or 270° in Fig. 3(a)] and minima along the hard axes (0° or 180°). In contrast, the angular dependence of coercivity shows additional symmetry. The multilayer exhibits coercivity minima along both the easy and hard axes. These two minima are separated by sharp peaks where the coercivity rises rapidly even a few degrees away from the hard axis. It is worth noting that the measurements had to be done with precision, otherwise the sharp angular variation in coercivity in the vicinity of the hard axis can be easily overlooked even with a slight misalignment of the applied field direction.

Figure 4 shows magnetization curves at various angles relative to the easy axis, corresponding to the broad minima in coercivity in Fig. 3(b). These curves show that magnetization changes in a highly stepwise manner and at comparable coercive fields. However, the extent of magnetization reversal by rotation increases at angles farther away from the easy axis, cf., Fig. 4(a) versus Fig. 4(d), causing remanence to decrease. In contrast, magnetization reversal along the hard

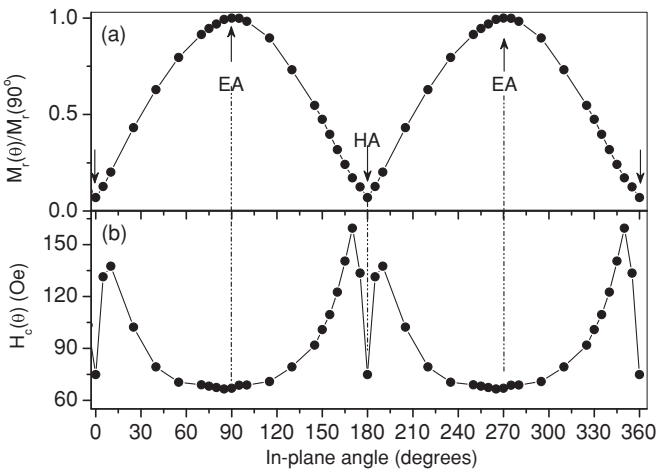

FIG. 3. Angular dependence of in-plane (a) remanence and (b) coercivity in TbFe/FeCo multilayer with 50 bilayers.

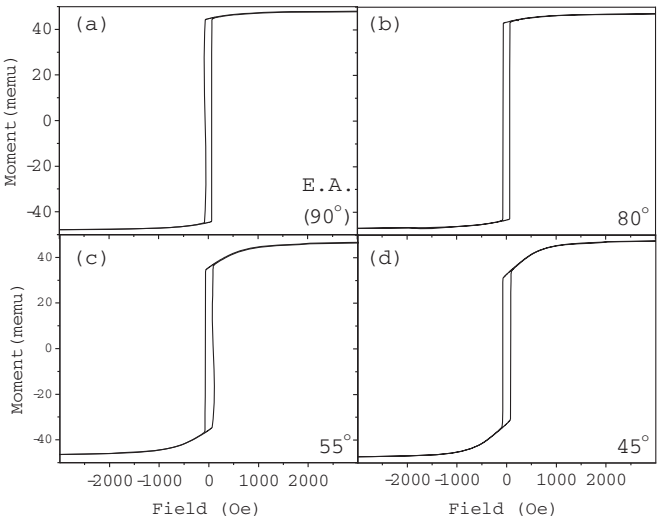

FIG. 4. In-plane hysteresis loops at various angles in the vicinity of the magnetic easy axis in TbFe/FeCo multilayer with 50 bilayers.

axis and at various angles away from it is dominated by rotation, as shown in Fig. 5. In particular, no stepwise change in magnetization is observed when the applied field is *precisely* along the hard axis, as shown in Fig. 5(a) or its zoom-in view in Fig. 6(a). Since magnetization along the hard axis occurs by rotation alone, *a priori*, domain walls are not expected to play any role during remagnetization. Remarkably, however, micromagnetic investigations revealed a new mode of reversal along the hard axis in these multilayers, one that is mediated by a domain wall even though reversal occurs entirely by rotation. This apparently counterintuitive process can be explained as follows. Figures 6(a_I)–6(a_{III}) show a sequence of micromagnetic images corresponding to the three arrows marked in Fig. 6(a). They show that at the point at which the slope of the magnetization curve changes [demarcated by the dotted lines in Fig. 6(a)], a domain wall nucleates and sweeps across the entire sample. The micrographs in Figs. 6(a_I)–6(a_{III})

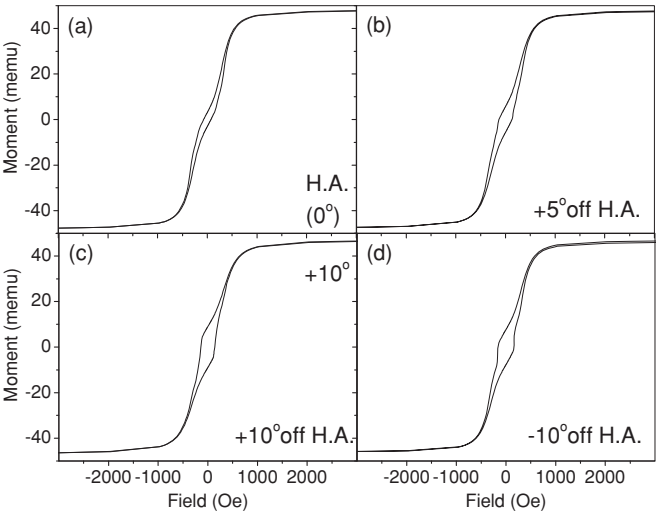

FIG. 5. In-plane hysteresis loops at various angles in the vicinity of the magnetic hard axis in TbFe/FeCo multilayer with 50 bilayers.

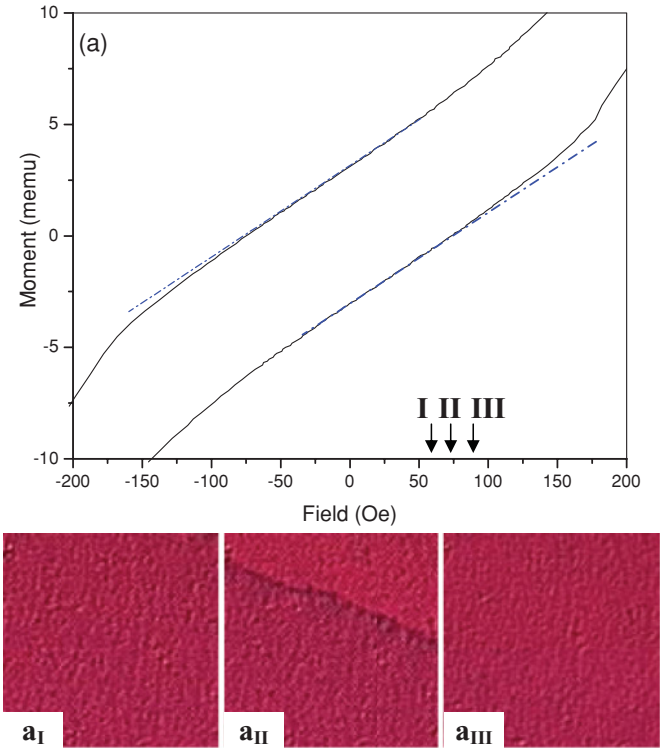

FIG. 6. (Color online) Zoom-in view of hysteresis loop along hard axis in TbFe/FeCo multilayer with 50 bilayers. (a_I)–(a_{III}) are the micromagnetic images corresponding to the fields at three respective arrows marked in (a).

were obtained by first saturating the sample in the negative direction, then reducing the field strength to zero, followed by increasing the field in the positive direction. An explanation for this behavior must reconcile the facts that reversal occurs by rotation, yet, a domain wall exists that does not register any stepwise change in the magnetization curve. As shown schematically in Fig. 7, consider magnetization to be initially aligned upwards along the hard axis in a sufficiently strong field. On reducing the field strength to zero, magnetization can possibly rotate either clockwise or counterclockwise as it spontaneously aligns itself along the easy axis, giving a net zero magnetization along the vertical direction (the direction of measurement). Both senses are equivalent and rotation occurs along both senses, and at zero field the sample subdivides itself into a self-consistent arrangement of magnetization fluctuations within a narrow cone angle about the easy axis, as shown in Fig. 7. As the sign of the applied field changes

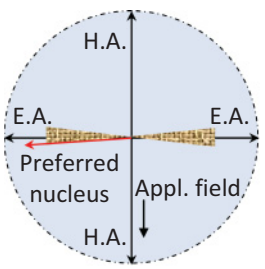

FIG. 7. (Color online) Schematic to explain the reversal mode along the hard axis in TbFe/FeCo multilayers. See text for explanation.

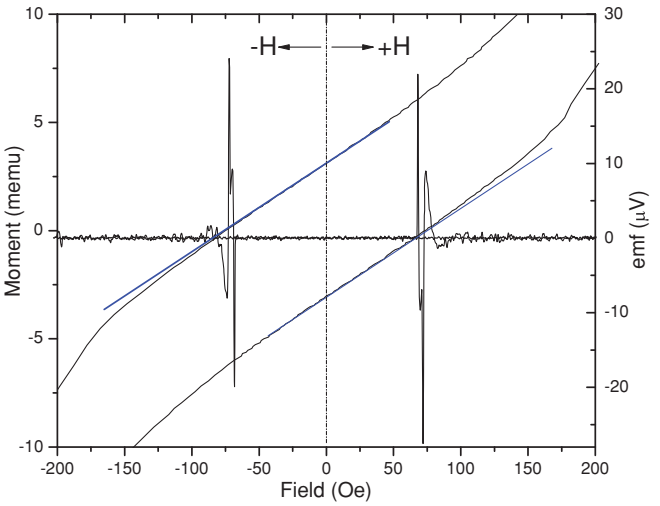

FIG. 8. (Color online) Induced emf signal in TbFe/FeCo multilayer with 50 bilayers for both the positive and the negative field cycles. The emf signal is superimposed on the zoomed-in magnetization curve along the hard axis to emphasize its correspondence with the points at which the slopes of the magnetization curve changes.

in the negative (downward) direction, at a critical field a preferred nucleus forms and grows to homogenize the entire sample into a single domain, as shown in Figs. 6(a_I)–6(a_{III}). At the same time, this process does not cause a stepwise change in magnetization along the hard axis since all magnetic fluctuations are already confined within the narrow cone angle along the easy axis (i.e., the net magnetization remains virtually unchanged due to the passage of this interface). Instead, the motion of the observed interface manifests itself as a small change in slope, as shown by deviation from linearity in Fig. 6(a). Next consider the dynamics of this interface. Figure 8 shows the emf signal emitted by the observed wall in Fig. 6(a_{II}) in both the positive and the negative field directions. The emf spikes in Fig. 8 are shown superimposed on the zoomed-in magnetization curve along the hard axis to emphasize its correspondence with the points at which the slopes of the magnetization curve changes. Although not shown, induction experiments were also carried out simultaneously with *in situ* observations of the micromagnetic structure, which further confirmed a direct correspondence between the emf signal and the passage of the domain wall under the pickup coil. The emf signature associated with the motion of this wall was found to be highly reproducible, as shown in Fig. 9(a) for ten consecutive field cycles; hundreds of such cycles were recorded. Figure 9(b) overlaps different field cycles to emphasize their reproducibility. The zoom-in view of the emf spike in the inset of Fig. 9(b) shows that the signal is in fact a composite of two closely spaced spikes of opposite polarity. Domain studies (discussed later) revealed that the composite spike arises from the lockstep motion of a twin wall, as shown in the inset of Fig. 9(b). The observed emf signal in the positive field direction was also found to be a mirror opposite of the signal in the negative field direction. Two examples of this are shown in Figs. 9(c) and 9(d), where the emf signals for positive and negative field cycles are plotted versus the absolute field values. In other words, the direction of

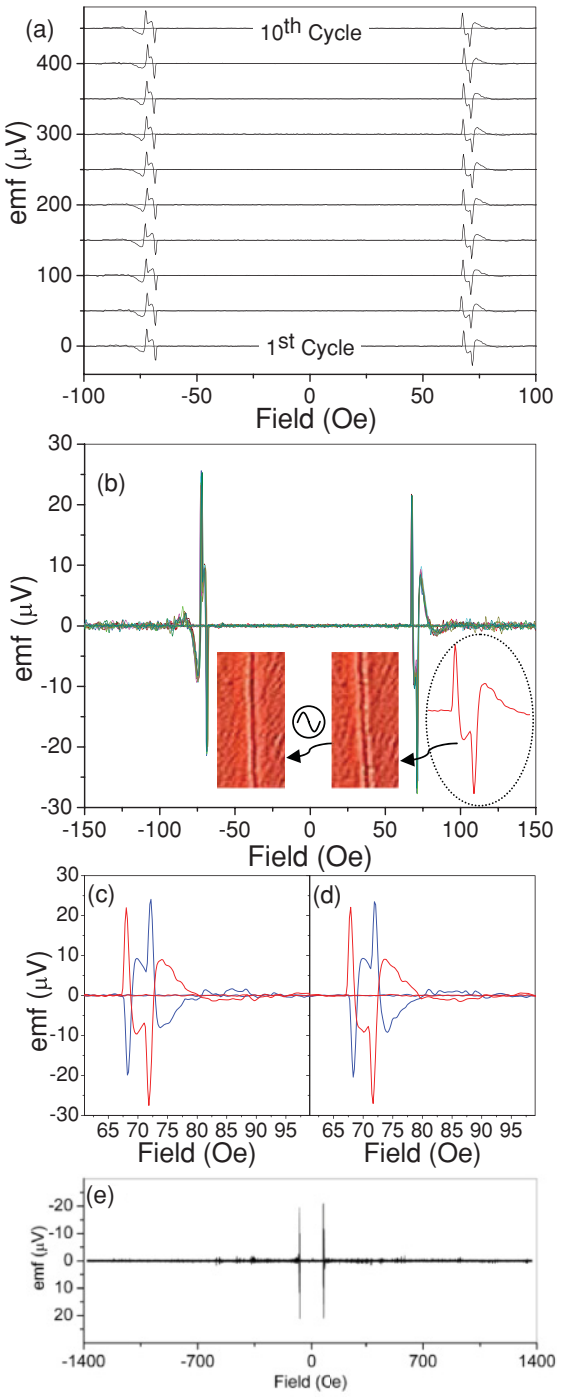

FIG. 9. (Color online) (a) Ten consecutive cycles showing emf signal along the hard axis for both positive and negative field cycles in TbFe/FeCo multilayer with 50 bilayers. Each cycle is offset by 50 μV. (b) The emf signal from consecutive cycles shown superimposed on each other to emphasize the reproducibility of avalanches. Inset shows the zoom-in profile of the emf spike. The right micrograph in the inset shows the twin domain wall whose motion causes the emf spike to occur. The left micrograph in the inset shows that the twin wall overlaps after the sample has been cycled in a small ac magnetic field (few oersted amplitude) superimposed on the static coercive field at which the twin wall appears. (c) and (d) Two examples of mirrorlike relation of emf signal for negative and positive fields, plotted as a function of absolute values of field. (e) The emf cycles over a larger field range.

the propagating interface (relative to the pickup coil) changes with the polarity of the applied field (say, from left to right in positive fields and *vice versa* in negative fields); this is also evident from Fig. 9(a). Also note that in Figs. 8 and 9, a small field range of less than ±200 Oe is shown simply to emphasize the reproducibility and profile of the emf signal. No wall motion occurs at higher fields, as shown in Fig. 9(e).

Next, consider the cooperative motion of the twin wall as a function of sweep rate. As described in the section on Experimental Details, for these experiments two pickup coils were placed on the sample 1.0 cm apart, and the time taken by the twin wall to sweep this distance was measured. Figure 10(a) shows the emf profile of the twin wall as it passes under the first coil (red trace) and then the second coil (green trace); as described in Sec. II, since the two pickup coils are rotated 180° relative to each other, notice the inverse polarity of the (red) emf signal in the first coil relative to the (green) emf signal in the second coil as the same wall sweeps across the sample. In addition, under acceleration, the twin wall can be seen moving at a higher velocity as it passes under the second pickup coil (higher amplitude). The twin wall gives twin peaks in the emf signal (A-B in red trace, and A′-B′ in the green trace). As shown in Fig. 10(a), wall A in the red trace takes time δt_1 to reach

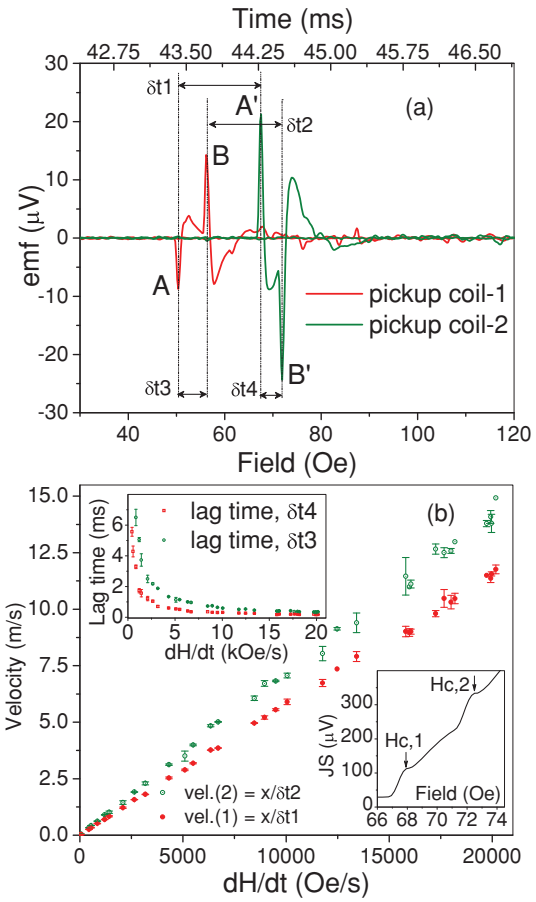

FIG. 10. (Color online) (a) The emf spikes due to the motion of a single twin wall across two pickup coils that are 1 cm apart. See text for explanation. (b) Linear response of twin walls versus driving rate. Inset in upper left plots lag times between two walls of twin wall at first and second pickup coils. Inset in lower-right plots JS versus field.

the second coil, whereas wall B takes time δt_2. The lag time between walls A and B under the first pickup coil is δt_3 whereas the lag time between walls A′-B′ is δt_4. Plotted as a function of sweep rate from 0.0001 Oe/s to ∼20 000 Oe/s, the twin wall shows a linear behavior for velocity, as shown in Fig. 10(b). Since wall B lags behind wall A in Fig. 10(a), it moves at higher velocities to keep up with wall B. The upper-left inset in Fig. 10(b) plots the lag times between walls A and B [δt_3] and between A′-B′ [δt_4] versus sweep rate. This inset shows that as the twin wall is accelerated at higher rates, the two wall segments show progressively greater overlap. At low sweep rates, the separation between the walls becomes larger, likely due to thermally induced creep just beyond the critical field for wall nucleation. The lower-right inset in Fig. 10(b) shows the jumpsum (JS) of the emf spike; the JS is simply the running total of emf versus field. The JS shows two distinct coercivity values for the twin wall segments, corresponding to the two different materials in the multilayer (TbFe and FeCo).

The emf signal assumes greater complexity in the form of multiple avalanches when the applied field is even a few degrees off the hard axis. This is shown in Fig. 11(a) corresponding to the hysteresis loop in Fig. 11(b), where the field is 15° off the hard axis; the inset in Fig. 11(b) is a zoom-in view of the magnetization curve. In Fig. 11(a), the red trace and the blue trace represent two successive cycles of applied field in the positive direction. To highlight reproducibility of spectra over these two successive cycles, the sign of the blue trace is algebraically reversed relative to the red trace. In contrast to a single avalanche along the hard axis in Fig. 9, magnetization reversal in Fig. 11(a) can be seen to occur by multiple avalanches. The insets show reproducibility of various avalanches from one cycle to another. Similarly, Fig. 11(c) shows a series of highly reproducible avalanches along the easy axis, corresponding to the hysteresis curve in Fig. 4(a).

Figures 12(a)–12(h) show micromagnetics of the lockstep motion of the twin wall along the easy axis, corresponding to the magnetization curve shown in Fig. 4(a). Following saturation in the negative direction, the field was reduced to zero, and then increased in the positive direction. Figure 12(a) shows the single domain state of the film, just prior to the appearance of a twin domain wall. The twin wall appears in the lower-right corner in Fig. 12(b) and moves towards the upper

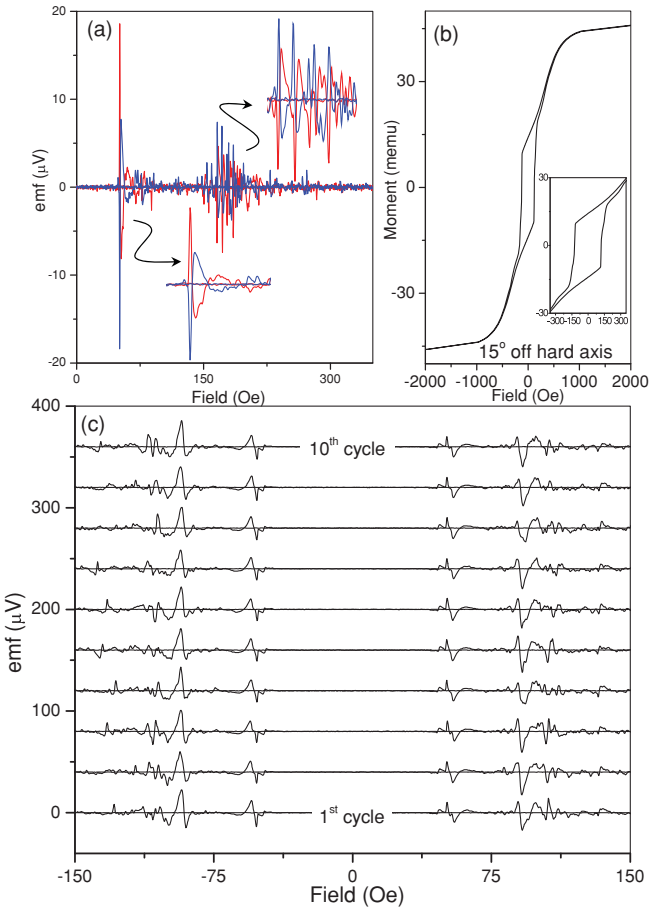

FIG. 11. (Color online) (a) Reproducible avalanches with applied field 15° off the hard axis. (b) Corresponding magnetization curve and its zoom-in view. (c) Examples of reproducible avalanches when the applied field is along the easy axis, corresponding to magnetization curve in Fig. 4(a). Ten complete consecutive cycles are shown. For each cycle, reproducible emf signal can be seen for both the positive and the negative field directions. Each cycle is offset by 50 μV.

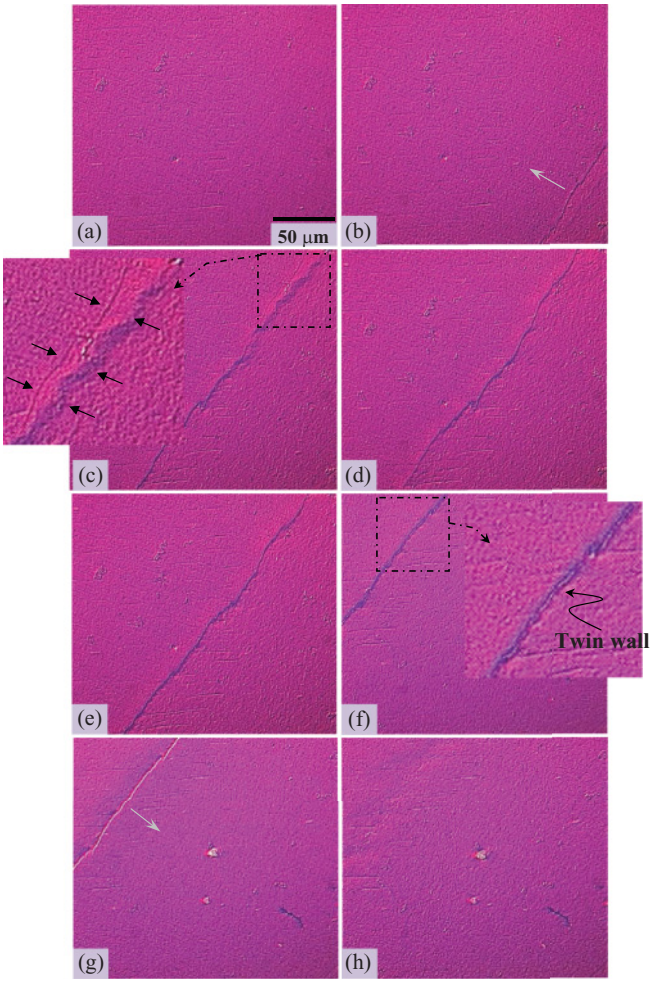

FIG. 12. (Color online) Micromagnetics associated with lockstep motion of coupled domain walls along the easy axis. Applied fields are (a) 55 Oe, (b) 57 Oe, (c) 72 Oe, (d) 81 Oe, (e) 80.9 Oe, (f) 80 Oe, (g) 29 Oe, (h) ∼−60 Oe. The applied field is close to the horizontal direction.

left as the field strength is increased, as shown in successive micrographs in Figs. 12(b)–12(f). The zoom-in view in Fig. 12(c) shows that the coupled walls momentarily become separated (due to a local defect), but overlap again, as shown in Fig. 12(d). The zoom-in view in Fig. 12(f) shows that the coupled wall has the configuration of a twin wall. In Fig. 12(f), the field strength is again reversed in order to move the twin wall backwards. Figures 12(g) and 12(h) show that this causes the polarity of the wall to be reversed as it begins to move toward the lower-right direction. Movie-1 in the supplemental material shows the entire process in greater detail.[73]

IV. DISCUSSION

Generally, the sequence of emf spikes in a Barkhausen spectrum bears no correlation to the sequence of spikes in successive field cycles (referred to as "lack of reproducibility" of Barkhausen spectra); no two sets of sequences are ever alike. This is because each time the sample is cycled in a magnetic field, magnetization reversal occurs randomly in numerous microscopic regions of the material. Not only do the volmes of these microscopic regions vary from one cycle to another, the sequence and rate at which it occurs is also random, thus giving a different spectrum each time the sample is cycled. However, a handful of insightful previous studies have shown limited reproducibility in small field excursions, in small samples, or over small distances.[74–79] The reproducibility of magnetic avalanches in the present study occurs along the entire major magnetization loop, and the same set of emf avalanches are reproducibly transmitted over macroscopic distances. The observed reproducibility has its origins in the highly synchronized and cooperative motion of domain walls in different layers. The cooperative motion of domain walls in these strongly exchange coupled multilayers as the basis for the observed reproducibility is contrasted with the behavior of a magnetic single film and a multilayer with weak interlayer

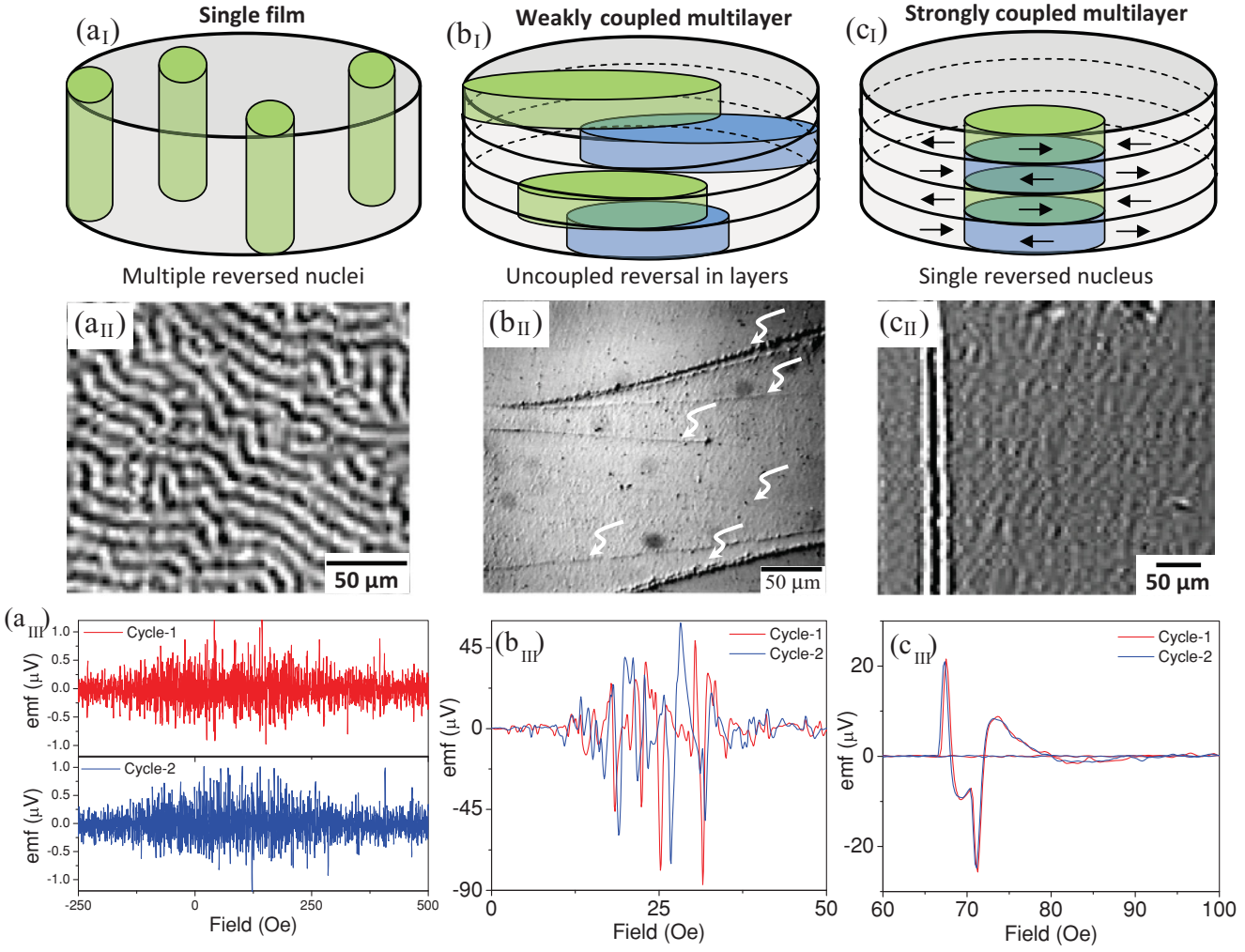

FIG. 13. (Color online) (a_I) Schematic showing a magnetic single film that undergoes magnetization reversal by growth of multiple domains. (a_{II}) The micromagnetic structure in an amorphous $Tb_{40}Fe_{60}$ single film. The film is 2.15 μm thick and has perpendicular anisotropy. (a_{III}) Barkhausen spectra for two consecutive cycles in the TbFe single film. (b_I) Schematic showing a magnetic multilayer with weak coupling. (b_{II}) The micromagnetic structure in a weakly coupled non-optimized multilayer {TbFe (7 nm)/FeCo (10 nm)} with 70 bilayers. (b_{III}) Barkhausen spectra for two consecutive cycles in TbFe/FeCo multilayer with weak coupling. (c_I) Schematic showing a magnetic multilayer with strong coupling. (c_{II}) The micromagnetic structure in a strongly coupled {TbFe (7 nm)/FeCo (10 nm)} with 50 bilayers. (c_{III}) Barkhausen spectra for two consecutive cycles in TbFe/FeCo multilayer with strong coupling.

coupling in Fig. 13. Figure 13(a_I) schematically shows a magnetic single film in which remagnetization occurs by the nucleation and growth of *multiple* reversed domains. This is shown in Fig. 13(a_{II}) for a TbFe film, where numerous mazelike reversed domains can be seen; the field-dependent behavior of such TbFe single films is discussed in detail elsewhere.[80] Each time the sample is cycled in a magnetic field, it emits a random sequence of voltage spikes due to a multitude of uncorrelated domain reversal processes in microscopic regions of the sample, as shown for two different cycles in Fig. 13(a_{III}). Next consider the case of a TbFe/FeCo multilayer. Since the Tb ions have negative exchange with Fe or Co ions, the larger moment of the Tb ion dominates within the Tb-Fe layer. In addition, the net moment of the Tb-Fe layer is antiparallel or ferrimagnetically aligned with the adjacent Fe-Co layers. If the adjacent layers are weakly coupled, reversed domains in different layers do not overlap on top of each other, as shown schematically in Fig. 13(b_I). Such a case is shown in Fig. 13(b_{II}) for a TbFe/FeCo multilayer with non-optimized deposition conditions, where nonoverlapping reversed domains in different layers are marked by the arrows; the micromagnetic behavior of such films is discussed in detail elsewhere.[61] As a result, there is limited coordination of domain-wall motion in different layers, which leads to limited reproducibility of the Barkhausen spectrum from one cycle to another, as shown in Fig. 13(b_{III}). Note that in contrast to the single film in Fig. 13(a_{II}), the number of voltage spikes in Fig. 13(b_{II}) is now greatly reduced, and their amplitude is greatly enhanced. Next consider the strongly exchange coupled TbFe/FeCo multilayer used in the present study. As discussed earlier, these multilayers undergo magnetization reversal by nucleation and motion of *a single twin wall across the entire area of the sample*. Moreover, since the adjacent layers are negatively exchange coupled, a reversed domain in one layer immediately triggers the nucleation of a corresponding reversed domain in adjacent layers, as shown schematically in Fig. 13(c_I). In other words, nucleation of a reversed domain in a given layer immediately triggers the nucleation of an entire set of reversed domains through the multilayer thickness. Once such a superstructure of stacked reversed domains is formed, it moves in unison, as shown in Fig. 13(c_{II}), where a twin wall can be seen. Due to the highly coordinated motion of a single twin wall, highly reproducible Barkhausen spectra are observed from one cycle to another, as shown in Fig. 13(c_{III}). Over repeated cycling, the same nuclei forms repeatedly and expands in the same defect environment. Also note the existence of a single avalanche in Fig. 13(c_{III}) in comparison to multiple spikes in Fig. 13(b_{II}), where reversal is seen to occur by a lesser choreographed motion of walls in different layers.

Finally, note that the reproducibility of the observed Barkhausen signal (a dynamic measurement) occurs by the lockstep motion of a *single* twin wall in the *same* defect environment as the sample being cycled between positive and negative saturation. It does not represent the average behavior of microscopic domains, and differs from previous work on so-called return-point memory, whose hallmark is the reversible return of a minor loop excursion onto the major loop. For interesting insight into return point memory effect, see for example, quasistatic x-ray speckle metrology studies in Refs. 81 and 82.

V. CONCLUSIONS

The reproducible magnetic avalanches along different in-plane directions are a result of highly synchronized motion of overlapping domain walls in different layers (twin wall). Reproducibility is possible since only a single twin wall moves across the entire macroscopic length of the sample. The dynamic studies also reveal a new mode of magnetization reversal along the hard axis in these multilayers, one that is mediated by a domain wall.

ACKNOWLEDGMENTS

This work was supported by the National Science Foundation, Grants No. DMR-0706074 and No. DMR-0305242, and this support is gratefully acknowledged. The authors acknowledge E. Quandt and A. Ludwig for some of the films used in the present study.

*Author to whom correspondence should be addressed: hchopra@buffalo.edu

[1] See *Out of the Crystal Maze: Chapters from the History of Solid-State Physics*, edited by Lillian Hoddeson, Ernest Braun, Jürgen Teichmann, and Spencer Weart (Oxford, New York, 1992), p. 382.
[2] H. Barkhausen, Phys. Z. **20**, 401 (1919).
[3] K. J. Sixtus and L. Tonks, Phys. Rev. **37**, 930 (1931).
[4] K. J. Sixtus and L. Tonks, Phys. Rev. **42**, 419 (1932).
[5] L. Tonks and K. J. Sixtus, Phys. Rev. **43**, 70 (1933).
[6] I. Langmuir and K. J. Sixtus, Phys. Rev. **38**, 2072 (1931).
[7] E. P. T. Tyndall, Phys. Rev. **24**, 439 (1924).
[8] R. M. Bozorth and J. F. Dillinger, Phys. Rev. **35**, 733 (1930).
[9] L. J. Swartzendruber, L. H. Bennett, H. Ettedgui, and I. Aviram, J. Appl. Phys. **67**, 5469 (1990).
[10] L. H. Bennett, L. J. Swartzendruber, I. Aviram, and I. I. Satija, J. Appl. Phys. **67**, 5350 (1990).
[11] L. B. Sipahi and D. C. Jiles, J. Magn. Magn. Mater. **104-107**, 385 (1992).
[12] L. B. Sipahi, D. C. Jiles, and D. Chandler, J. Appl. Phys. **73**, 5623 (1993).
[13] L. J. Swartzendruber, G. E. Hicho, H. D. Chopra, S. D. Leigh, G. Adam, and E. Tsory, J. Appl. Phys. **81**, 4263 (1997).
[14] S. Zapperi, P. Cizeau, G. Durin, and H. E. Stanley, Phys. Rev. B **58**, 6353 (1998).
[15] E. Puppin, Phys. Rev. Lett. **84**, 5415 (2000).
[16] G. Durin and S. Zapperi, Phys. Rev. Lett. **84**, 4705 (2000).
[17] S. Yang and J. L. Erskine, Phys. Rev. B **72**, 064433 (2005).
[18] M. Liebmann, A. Schwarz, U. Kaiser, R. Wiesendanger, D.-W. Kim, and T.-W. Noh, Phys. Rev. B **71**, 104431 (2005).
[19] D. A. Christian, K. S. Novoselov, and A. K. Geim, Phys. Rev. B **74**, 064403 (2006).
[20] O. Perevertov, J. Phys. D **40**, 949 (2007).

[21]M. Kupferling, F. Fiorillo, V. Basso, G. Bertotti, and P. Meilland, J. Magn. Magn. Mater. **320**, E527 (2008).
[22]Z. Diao, E. R. Nowak, G. Feng, and J. M. D. Coey, Phys. Rev. Lett. **104**, 047202 (2010).
[23]N. Abu-Libdeh and D. Venus, Phys. Rev. B **81**, 195416 (2010).
[24]C. W. Heaps, Phys. Rev. **50**, 176 (1936).
[25]G. Bonfiglioli, A. Ferro, G. Montalenti, and G. Rosa, Phys. Rev. **94**, 316 (1954).
[26]R. C. O'Handley, J. Appl. Phys. **46**, 4996 (1975).
[27]C. H. Tsang, R. L. White, and R. M. White, J. Appl. Phys. **49**, 1838 (1978).
[28]R. P. D. Real, C. Prados, D.-X. Chen, A. Hernando, and M. Vazquez, Appl. Phys. Lett. **63**, 3518 (1993).
[29]H. Chiriac, T. A. Óvári, and Gh. Pop, Phys. Rev. B **52**, 10104 (1995).
[30]D. X. Chen, N. M. Dempsey, M. Vazquez, and A. Hernando, IEEE Trans. Magn. **31**, 781 (1995).
[31]J. Velázquez, C. García, M. Vázquez, and A. Hernando, Phys. Rev. B **54**, 9903 (1996).
[32]M. R. Sullivan, A. A. Shah, and H. D. Chopra, Phys. Rev. B **70**, 094428 (2004).
[33]R. Varga, K. L. Garcia, M. Vázquez, and P. Vojtanik, Phys. Rev. Lett. **94**, 017201 (2005).
[34]H. D. Chopra and M. R. Sullivan, Rev. Sci. Instrum. **76**, 013910 (2005).
[35]R. L. Novak, J. P. Sinnecker, and H. Chiriac, J. Phys. D **41**, 095005 (2008).
[36]M. Ipatov, V. Zhukova, A. K. Zvezdin, and A. Zhukov, J. Appl. Phys. **106**, 103902 (2009).
[37]M. Ipatov, V. Zhukova, A. Zvezdin, J. Gonzalez, J. M. Blanco, and A. Zhukov, J. Supercond. Novel Magn. doi: 10.1007/s10948-010-1029-9 (2010).
[38]See review, A. Yelon, in *Physics of Thin Films*, edited by M. H. Francombe and R. W. Hoffman (Academic, New York, 1971), Vol. 6, p. 205.
[39]H. Clow, Nature (London) **194**, 1035 (1962).
[40]S. Middelhoek, Z. Angew. Phys. **18**, 524 (1965).
[41]S. Middelhoek, IBM J. Res. Dev. **9**, 147 (1965).
[42]J. C. Slonczewski and S. Middelhoek, Appl. Phys. Lett. **6**, 139 (1965).
[43]F. Biragnet, J. Devenyi, G. Clerc, O. Massenet, R. Montmory, and A. Yelon, Phys. Status Solidi B **16**, 569 (1966).
[44]E. Feldtkeller, J. Appl. Phys. **39**, 1181 (1968).
[45]H. Niedoba, A. Hubert, B. Mirecki, and I. B. Puchalska, J. Magn. Magn. Mater. **80**, 379 (1989).
[46]S. Z. Hua, D. S. Lashmore, L. J. Swartzendruber, J. W. F. Egelhoff, K. Raj, and H. D. Chopra, J. Appl. Phys. **81**, 4582 (1997).
[47]H. D. Chopra, M. R. Sullivan, A. Ludwig, and E. Quandt, Phys. Rev. B **72**, 054415 (2005).
[48]T. Zimmermann, J. Zweck, and H. Hoffmann, J. Magn. Magn. Mater. **149**, 409 (1995).
[49]L. J. Heyderman, J. N. Chapman, and S. S. P. Parkin, J. Magn. Magn. Mater. **138**, 344 (1994).
[50]I. Tomeš, H. Niedoba, M. Rührig, G. Wittmann, A. Hubert, H. O. Gupta, L. J. Heyderman, and I. B. Puchalska, Phys. Status Solidi A **128**, 203 (1991).
[51]V. S. Speriosu, B. Dieny, P. Humbert, B. A. Gurney, and H. Lefakis, Phys. Rev. B **44**, 5358 (1991).
[52]B. Dieny, V. S. Speriosu, S. S. P. Parkin, B. A. Gurney, D. R. Wilhoit, and D. Mauri, Phys. Rev. B **43**, 1297 (1991).
[53]B. Dieny, J. Magn. Magn. Mater. **136**, 335 (1994).
[54]T. C. Anthony, J. A. Brug, and Z. Shufeng, IEEE Trans. Magn. **30**, 3819 (1994).
[55]H. D. Chopra, D. X. Yang, P. J. Chen, D. C. Parks, and W. F. Egelhoff, Phys. Rev. B **61**, 9642 (2000).
[56]E. F. Kneller and R. Hawig, IEEE Trans. Magn. **27**, 3588 (1991).
[57]E. Quandt, A. Ludwig, J. Betz, K. Mackay, and D. Givord, J. Appl. Phys. **81**, 5420 (1997).
[58]E. Quandt, A. Ludwig, D. G. Lord, and C. A. Faunce, J. Appl. Phys. **83**, 7267 (1998).
[59]M. Wuttig, Q. Su, F. Masson, E. Quandt, and A. Ludwig, J. Appl. Phys. **83**, 7264 (1998).
[60]E. Quandt and A. Ludwig, J. Appl. Phys. **85**, 6232 (1999).
[61]H. D. Chopra, A. Ludwig, E. Quandt, S. Z. Hua, H. J. Brown, L. J. Swartzendruber, and M. Wuttig, J. Appl. Phys. **85**, 6238 (1999).
[62]H. D. Chopra, D. X. Yang, and P. Wilson, J. Appl. Phys. **87**, 5780 (2000).
[63]D. T. H. Giang, N. H. Duc, V. N. Thuc, L. V. Vu, and N. Chau, Appl. Phys. Lett. **85**, 1565 (2004).
[64]J.-P. Jay, F. Petit, J. B. Youssef, M. V. Indenbom, A. Thiaville, and J. Miltat, J. Appl. Phys. **99**, 093910 (2006).
[65]M. Gonzalez-Guerrero, J. L. Prieto, D. Ciudad, P. Sanchez, and C. Aroca, Appl. Phys. Lett. **90**, 162501 (2007).
[66]C. Favieres, J. Vergara, and V. Madurga, J. Phys. D. **40**, 4101 (2007).
[67]U. Hartmann and H. H. Mende, J. Phys. D **18**, 2285 (1985).
[68]C. Bathany, M. Le Romancer, J. N. Armstrong, and H. D. Chopra, Phys. Rev. B **82**, 184411 (2010).
[69]M. R. Sullivan and H. D. Chopra, Phys. Rev. B **70**, 094427 (2004).
[70]J. N. Armstrong, M. R. Sullivan, M. Le Romancer, V. A. Chernenko, and H. D. Chopra, J. Appl. Phys. **103**, 023905 (2008).
[71]M. R. Sullivan, D. A. Ateya, S. J. Pirotta, A. A. Shah, G. H. Wu, and H. D. Chopra, J. Appl. Phys. **95**, 6951 (2004).
[72]F. Bitter, Phys. Rev. **38**, 1903 (1931).
[73]See supplemental material at [http://link.aps.org/supplemental/10.1103/PhysRevB.83.054426] for Movie-1 showing the lockstep motion of a twin wall.
[74]J. Horvat, E. Babic, and Z. Marohnic, J. Magn. Magn. Mater. **86**, L1 (1990).
[75]C. D. Keener and M. B. Weissman, Phys. Rev. B **51**, 11463 (1995).
[76]J. S. Urbach, R. C. Madison, and J. T. Markert, Phys. Rev. Lett. **75**, 4694 (1995).
[77]J. R. Petta, M. B. Weissman, and K. P. O'Brien, Phys. Rev. E **54**, R1029 (1996).
[78]J. R. Petta, M. B. Weissman, and G. Durin, Phys. Rev. E **56**, 2776 (1997).
[79]P. Plewka, J. J. Zdotebrowski, and M. Urbanacuteski, Phys. Rev. E **57**, 6422 (1998).
[80]C. Bathany, M. Le Romancer, J. N. Armstrong, and H. D. Chopra, Phys. Rev. B **82**, 184411 (2010).
[81]M. S. Pierce, R. G. Moore, L. B. Sorensen, S. D. Kevan, O. Hellwig, E. E. Fullerton, and J. B. Kortright, Phys. Rev. Lett. **90**, 175502 (2003).
[82]M. S. Pierce *et al.*, Phys. Rev. Lett. **94**, 017202 (2005).